Soft Matter

View Online
Dynamic Article Links

Cite this: *Soft Matter*, 2011, **7**, 8330

www.rsc.org/softmatter

PAPER

Reflection and exclusion of shear zones in inhomogeneous granular materials

Tamás Börzsönyi,*[a] Tamás Unger,[b] Balázs Szabó,[a] Sandra Wegner,[c] Frank Angenstein[d] and Ralf Stannarius[c]

Received 26th April 2011, Accepted 17th June 2011
DOI: 10.1039/c1sm05762f

Published on 05 August 2011 on http://pubs.rsc.org | doi:10.1039/C1SM05762F
Downloaded by Otto von Guericke Universitaet Magdeburg on 07 October 2011

Shear localization in granular materials is studied experimentally and numerically. The system consists of two material layers with different effective frictions. The presence of the material interface leads to a special type of "total internal reflection" of the shear zone. In a wide range of configurations the reflection is characterized by a fixed angle which is analogous to the critical angle of refraction in optics. The zone leaves and reenters the high friction region at this critical angle and in between it stays near the interface in the low friction region. The formalism describing the geometry of the shear zones and that of refracted and reflected light beams is very similar. For the internal visualization of shear localization two independent experimental techniques were used (i) excavation and (ii) magnetic resonance imaging.

1 Introduction and model

Shearing of complex materials, *e.g.* non-newtonian fluids, colloids, emulsions, foams or granular materials, often leads to shear localization.[1–6] The region with the highest shear rate is called the shear zone (or shear band).[7–21] Experiments and numerical simulations for granular materials showed that the shear zone can exhibit nontrivial curved or refracted shapes even for the simplest stationary case, where the position and shape of the shear zone remains more or less the same during the shear deformation.[5–13] The case of inhomogeneous materials is especially important for understanding various natural phenomena or industrial problems. In such systems, where the internal friction of the material changes with location, the shear is preferentially localized to regions with lower friction. A simple example is the case of a layered material where different layers correspond to different friction – a configuration which is often seen in nature. The aim of the current paper is to characterize the puzzling shapes of shear zones in such systems by experimental and numerical techniques.

The shape of the shear zone can be captured by a simple variational model[10,22] where the basic idea is the following: the shear zone is modeled as an infinitely thin sliding surface. For any potential sliding surface that is consistent with the boundary conditions, one has to determine its total shear resistance against the driving. The actual shear zone will correspond to the sliding surface that has the lowest total resistance. This is the weakest surface that yields first and separates the system into two solid blocks that slide next to each other. The protocol for the determination of the shear resistance depends on the actual configuration. On one hand, for Couette or cylindrical split-bottom shear cells the potential sliding surfaces are loaded by the same mechanical *torque*. Therefore the weakest surface has to be determined based on the ability to transmit the torque. On the other hand, if straight shear cells are used as in the present study, the potential sliding surfaces experience an equal shear *force*. Therefore the shear zone will correspond to the potential sliding surface that is the weakest regarding its ability to transmit the total shear force between its two sides. In both cases – described by minimum torque or minimum force – the shear deformation corresponds to the lowest possible energy dissipation.[10,22]

In this paper we deal with straight shear cells where shearing is provided by the relative motion of two long parallel sliders (Fig. 1 and 2). Then the shear zone is created between two material blocks, each stuck to one of the sliders. The location of the emerging shear zone can be determined by the above consideration. As the geometry is translation invariant in the direction of shear (x direction) the shear zone can be represented by a single path in the cross section of the cell (yz plane). The total shear force that can be transmitted by such a path is proportional to the integral

$$\int \tau \, \mathrm{d}s = \min, \tag{1}$$

where τ, the maximum shear stress that the material can exert locally, is integrated along the length s of the path. The shear zone corresponds to the path for which the integral takes its minimum value. It is assumed that τ is given by the product of the effective friction coefficient μ and the local pressure† p

$$\tau = \mu p. \tag{2}$$

[a]*Research Institute for Solid State Physics and Optics, P.O. Box 49, H-1525 Budapest, Hungary. E-mail: btamas@szfki.hu; Fax: +36 1 3922215; Tel: +36 1 3922222*
[b]*HAS-BUTE Condensed Matter Research Group, Budapest University of Technology and Economics, H-1111 Budapest, Hungary*
[c]*Institute of Experimental Physics, Otto von Guericke University, Universitätsplatz 2, D-39106 Magdeburg, Germany*
[d]*Leibniz Institute for Neurobiology, D-39118 Magdeburg, Germany*

† We neglect here, that the stress tensor is not spherical.

This journal is © The Royal Society of Chemistry 2011

View Online

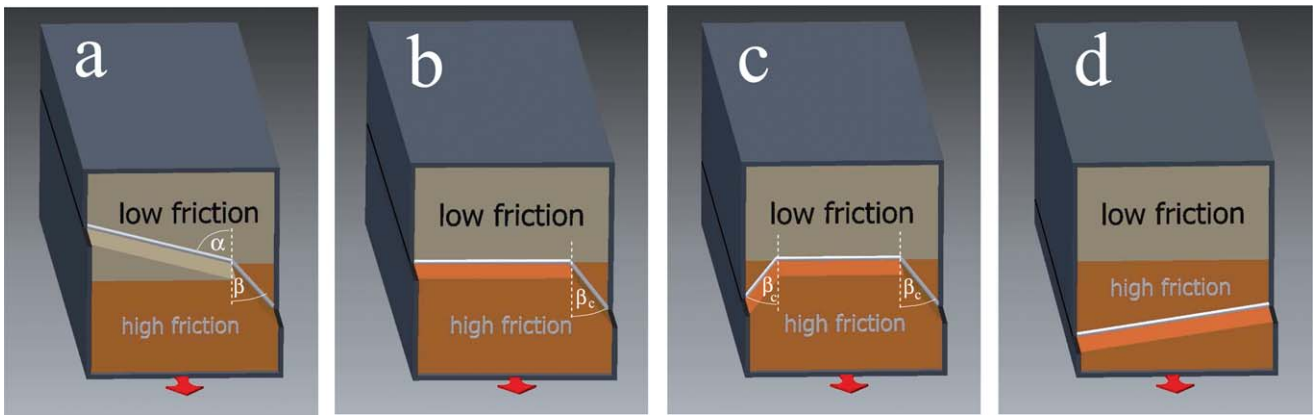

Fig. 1 A gedankenexperiment: a material consisting of two layers is sheared by moving the bottom part of the cell according to the red arrow. The four panels illustrate how the boundary conditions affect the position of the shear zone in this closed system. From (a) to (d) the left boundary of the zone (position of the slider edges) is moved downwards step by step, whereas its right boundary is kept fixed. The case (a) is analogous to the refraction of light beams. (b) Limit angle of refraction β_c. Panel (c) shows the "total reflection" of the shear zone. It is quite different from the total reflection of geometric optics as part of the zone is excluded from the high friction material and the zone arrives at the interface at the limit angle β_c. (d) Straight zone, not influenced by the interface.

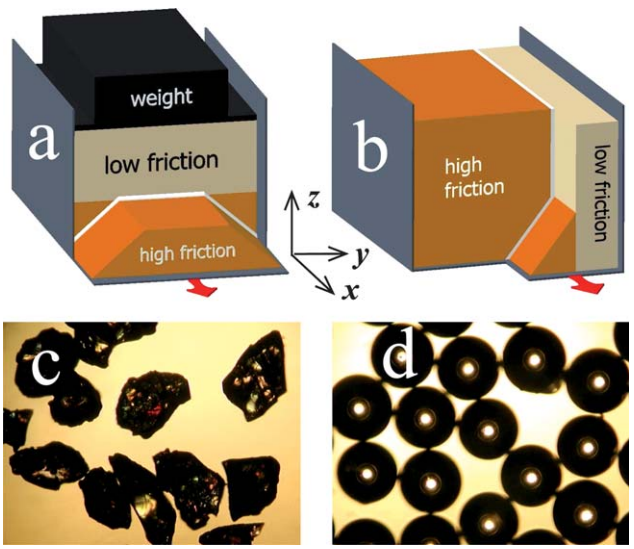

Fig. 2 (a)–(b) Schematic illustration of the two experimental configurations used. The layered granular material is sheared by moving (a) the lower boundary for the "*closed system*" or (b) one of the L-shaped walls for the "*open system*" according to the red arrow. The location of the shear zone is indicated with a white line. The upper surface of the "*closed system*" is loaded with a weight 3 times heavier than the granular material below. (c) and (d) Microscopic images of the materials used in the experiments: (c) corundum (grain size $d = 0.33 \pm 0.02$ mm) and (d) glass beads (grain size $d = 0.48 \pm 0.02$ mm).

In an inhomogeneous system the effective friction μ can vary from place to place, *e.g.* when layers of different materials are present. When p is constant, the condition (1) reduces to $\int \mu \, ds = \min$, which is formally identical to the well-known Fermat principle in optics. According to this, the light beam traveling through an optically inhomogeneous material finds the optimal way, where the length weighted by the refraction index is extremal. This results in refraction of light beams at the boundaries of regions with different optical indices. The analogy leads to the idea that similar refraction effects are expected in these two distant fields of physics. The case of zone refraction can then be described by a law which is similar to the refraction law in optics

$$\frac{\sin\alpha}{\sin\beta} = \frac{\mu_h}{\mu_l},$$

where α and β are the two angles of incidence (see Fig. 1a), while μ_l and μ_h stand for the effective friction in the two layers with low friction and high friction, respectively. This law was recently tested numerically and experimentally.[10–13]

In the present work we do not deal with the case of refraction but focus on configurations in which the zone after visiting the interface eventually returns to the high friction part of the sample. The boundary conditions, where both ends are located in the high friction material, correspond to the total internal reflection in geometric optics. However, in this situation the behavior of the shear zone differs from the behavior of light beams (Fig. 1c). Our version of Fermat's principle, *i.e.* the global minimum of $\int \mu \, ds$, suggests the following interesting scenario. Here the middle part of the shear zone is excluded from the high friction material and it is located as close as possible to the interface but in the low friction region. Thus this part of the zone enters with the coefficient μ_l into the calculation of the total transmitted shear force. The shear zone from both sides reaches the interface at the critical angle β_c defined by $\sin\beta_c = \mu_l/\mu_h$. Interestingly this angle characterizes a wide range of configurations not only the limit case of refraction (Fig. 1b).

It can be easily verified that the above exclusion effect and the piecewise straight shape of the shear zone (Fig. 1c) indeed corresponds to the least possible shear force within the framework of the variational model of the infinitely narrow zone. In the following we test this picture experimentally.

2 Experimental methods

For the experimental realization of the above described systems we use two materials with different frictional properties. One

Downloaded by Otto von Guericke Universitaet Magdeburg on 07 October 2011
Published on 05 August 2011 on http://pubs.rsc.org | doi:10.1039/C1SM05762F

View Online

Downloaded by Otto von Guericke Universitaet Magdeburg on 07 October 2011
Published on 05 August 2011 on http://pubs.rsc.org | doi:10.1039/C1SM05762F

material is corundum which consists of angular grains (see Fig. 2c). Therefore it has higher effective internal friction than the other material consisting of glass beads (Fig. 2d). To characterize the difference in the effective frictions, the angles of repose (θ_r) were determined by the method used in[23] and were $\theta_r^{gla} = 21.9^\circ$ for glass beads while $\theta_r^{cor} = 33.2^\circ$ for corundum. The latter is somewhat higher than the typical value for sand ($\theta_r^{san} = 30.5^\circ$). The effective frictions are simply estimated by $\mu \approx \tan\theta_r$. The ratio $\tan\theta_r^{cor}/\tan\theta_r^{gla} = 1.63$ gives a reasonable contrast for the effective friction.

Two experimental geometries were investigated. In the first one – which is referred to as "*closed system*" (see Fig. 2a) – the zone was forced to start and end in the high friction part of the sample. Here the granular materials were layered horizontally with the low friction material placed on top of the high friction material and shearing was obtained by a slow translation of the bottom plate according to the red arrow. If the thickness of the lower (high friction) layer is not too large the zone escapes it and then comes back to it, as indicated by the white line. In order to reduce the relative pressure difference between the top and bottom of the system the upper surface was loaded with a weight which was about 3 times heavier than the granular material below. The length of the cell was 70 cm and it had an internal cross section of 4.5 cm × 4 cm.

The second experimental apparatus referred to as "*open system*" (see Fig. 2b) included two 70 cm long L-shaped sliders (cell wall), one of which was slowly translated in the experiments. When the two granular layers (with low and high friction) are arranged vertically (as seen on the sketch), the shear zone takes a form as it is indicated by the white line. It is forced to start in the high friction part of the sample but is free to select the position of the other end at the top surface. This cell had an internal cross section of 4 cm × 3.5 cm. The total shear displacement achieved in each experiment was between 5 and 6 cm for both cases (Fig. 2a and 2b).

Two methods were used for the measurement of the deformation: (i) using colored samples and excavating the material layer by layer (see Fig. 3) the displacement was detected optically by digital imaging and (ii) the whole cell was placed into a magnetic resonance imaging (MRI) apparatus and the displacement was detected by tracer particles (see Fig. 4). In the following we demonstrate both methods.

In the case of optical detection we used two samples with different colors each for both materials. In the upper layer, brown and gray correspond to glass beads (grain sizes $d = 0.56 \pm 0.02$ mm and $d = 0.48 \pm 0.02$ mm), while in the bottom layer, dark blue and white correspond to corundum (grain sizes $d = 0.33 \pm 0.02$ mm and $d = 0.23 \pm 0.02$ mm). After each experiment the material was carefully removed layer by layer[9,12] and the displacement profile $D(y)$ was determined for each horizontal layer as it is illustrated by sample images in Fig. 3a. We used a commercial vacuum cleaner with additional extension tubes to provide a slow flow rate. The procedure takes several hours for one experiment. Typically 20–25 layers were recorded with the smallest interslice distance of 1 mm. The $D(y,z)$ displacement profile shown in Fig. 3b resulted after combining the information obtained for all slices.

Visualization of the internal deformation of the material by magnetic resonance imaging was realized using a Bruker BioSpec 47/20 MRI scanner operating at 200 MHz proton resonance frequency (4.7 T) at the Leibniz Institute for Neurobiology, Magdeburg. The cross section of our experimental apparatus was optimized for the geometry of this device with 7 cm internal coil diameter. Since the granular samples used (corundum and glass beads) do not give an MRI signal, tracer particles were needed. The tracer particles should be large enough allowing the detection of single particles, but also not too large for the best spatial resolution. The best signal was obtained using poppy seeds with the size of $d = 0.75 \pm 0.04$ mm). Similarly to the case of excavation horizontal slices were obtained with the interslice distance of 0.8 mm and the in plane resolution of 0.156 mm per pixel. The slider was displaced by 2.5 mm between subsequent

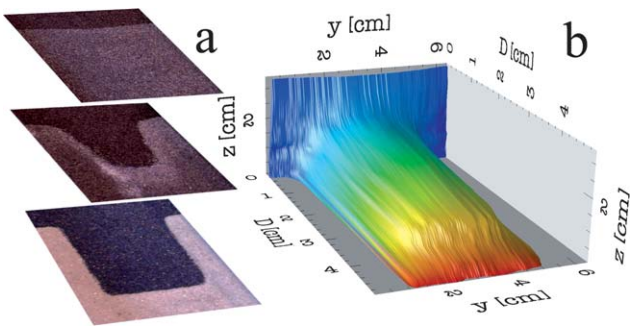

Fig. 3 Demonstration of the excavation method for the case of the *closed system*. (a) Sample images taken during excavation. The displacement of the grains inside the sample is visualized by carefully removing the material layer by layer. (b) Displacement $D(y,z)$. The position of the interface between the two materials was at height 1.0 cm.

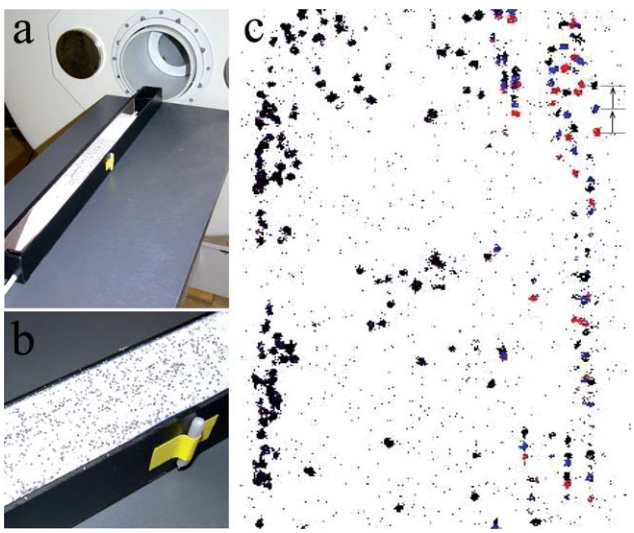

Fig. 4 Demonstration of the measurements using magnetic resonance imaging for the case of the *open system*. (a)–(b) The experimental cell filled with the material doped with poppy seeds. (c) Overlapped horizontal sample images taken at $z = 3.2$ cm. Poppy seeds appear as distinct spots on the binarized images with different colors for the 3 subsequent images. As expected, only the right hand side of the material is moving (see Fig. 2b), and the shear zone is shifted to the right with respect to the cell middle.

 This journal is © The Royal Society of Chemistry 2011

View Online

MRI scans, Fig. 4c shows 3 subsequent images overlapped taken at $z = 3.2$ cm. During one experiment 20–30 displacement steps were recorded yielding a total displacement of 5–7.5 cm. The total measurement took about 4 h. We note, that a potential segregation of the tracers during shear if present, would be immediately evident in the MRI images. Such segregation played no role in the present experiments.

3 Simulation method

The computer simulations presented here are based on the variational narrow band model that we summarized in the introduction. However, the simulation tries to overcome one serious drawback of the narrow band model, namely that it regards the shear zone as infinitely thin. In reality the zone has a non-negligible finite width and the system has a smooth shear profile. In the simulation, wide shear zones are achieved by introducing fluctuations due to disorder of the granular material as follows. For a given state of the system, *i.e.* for one random realization of the material, we identify the weakest sliding surface according to the variational narrow band model (details are given below). This procedure can be repeated many times for various random realizations which results in a large number of narrow shear bands. Taking an ensemble average over the random realizations provide us with a smooth shear profile and a wide shear zone. A justification of this approach can be seen in the three-dimensional structure of the actual shear zone. It adopts an averaged profile in the yz cell cross section by averaging over all slices along the x direction.

Such a protocol has been first used in computer simulations performed by Török *et al.*,[8] however, there are two major differences between those simulations and the present method. First, here we use independent random realizations as opposed to the self-organized random potential used earlier.[8] Second, the square lattice that was used in the previous studies[8] inevitably introduces preferred orientations for the shear zone. It is important that we avoid such a bias. Therefore here an isotropic random mesh is used instead of a regular lattice.

The two-dimensional random mesh is generated in the yz cross section of the system perpendicular to the shear direction. First, we start with the grid points of a square lattice (without bonds) of lattice constant a. Second, the position of each point is regenerated in a square of size $2a \times 2a$ which is centered on the original position of the point. The new random position is then chosen uniformly inside the square. In the third step the points are connected with bonds using Delaunay triangulation (Fig. 5). The resulting mesh is macroscopically isotropic to a good approximation. For example testing the bond orientations shows that all directions are equally probable and we found no sign of the orientation of the original square lattice.

The triangles of the mesh correspond to microscopic blocks of the material while bonds represent interfaces between the blocks where sliding can take place. The maximum shear force‡ S that a given bond can exert without sliding is given by $l\mu pR$, where l is the length of the bond, μ is the local coefficient of the effective friction, p is the local pressure and R is a random number chosen uniformly between 0 and 1. Each bond has its own random number R that is regenerated for each random realization of the material. It is assumed that the local pressure p is hydrostatic, *i.e.* p is proportional to the weight of the material above.

‡ In fact, the quantity S calculated here has the meaning of shear force per unit length in x-direction.

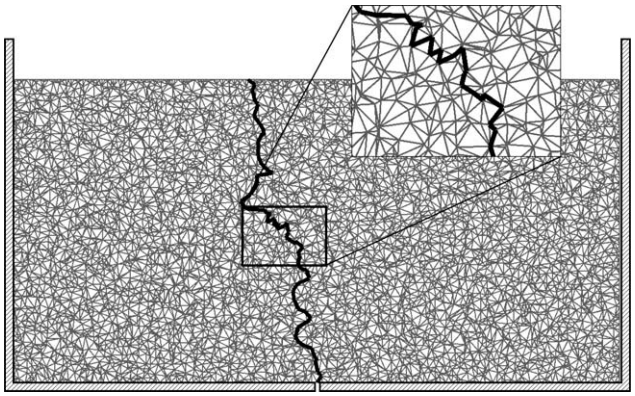

Fig. 5 The random mesh used by the MC simulation and one shear band. This situation corresponds to the straight split bottom cell filled with one material. The band starts at the split line of the bottom and ends at the free top surface of the system. The shear band represents the weakest sliding surface for the given random realization of the material.

Any potential sliding surface which is consistent with the boundary conditions can now be represented by a continuous chain of bonds. For example the two ends of the chain are fixed for the closed system according to Fig. 2a, while for the open system (Fig. 2b) only the lower end is fixed at the split line of the boundary, the upper end is free, *i.e.* it can be anywhere at the top surface of the material. For such a chain Γ the total shear force that it can resist is given by the sum of bond forces S_i for all the bonds i contained in Γ. The actual shear band Γ, *i.e.* the weakest sliding surface, is determined by the condition

$$\sum_{i\in\Gamma} l_i\mu_i p_i R_i = \min. \qquad (3)$$

The shape of the shear band depends on the actual random realization. Such a shear band represents a displacement jump and therefore a noncontinuous displacement field. It divides the material into two regions: the region on one side of the shear band has a unit shear displacement in x-direction while the region on the other side has zero displacement.

In our Monte Carlo simulation we generate shear bands for many random realizations (typically a couple of thousand bands are collected). The displacement field that is obtained by averaging over random realizations is continuous and can be directly compared to the experimental displacement profiles.

The local friction coefficients μ_i are set according to the experimentally measured values. There is only one free parameter left in the simulation, namely the resolution of the mesh based on the lattice constant a. The parameter a has to be calibrated once for each type of material. This has been done with the help of the straight split bottom cell using only a single material and by matching the width of the shear zone between simulation and experiment. This provided us with calibration ratios between grain size d and lattice constant a. We obtained $a/d = 0.42$ for glass beads, and $a/d = 0.11$ for corundum. This is in accordance with other measurements on homogeneous materials[6] showing that the

Downloaded by Otto von Guericke Universitaet Magdeburg on 07 October 2011
Published on 05 August 2011 on http://pubs.rsc.org | doi:10.1039/C1SM05762F

View Online

Downloaded by Otto von Guericke Universitaet Magdeburg on 07 October 2011
Published on 05 August 2011 on http://pubs.rsc.org | doi:10.1039/C1SM05762F

thickness of the zone is larger for spherical beads than for irregular grains. This also means that in the simulations of the inhomogeneous systems presented in this paper a is not constant in space. The applied resolution of the underlying mesh is different for the different materials. After this calibration is done there is no fit parameter left in the simulation method.

4 Results

We first present the results obtained for the *closed system* using excavation. The final displacement $D(y,z)$ of the material is presented in Fig. 6a–d for four measurements in such a way that regions with highest shear deformation are visualized. As it is seen both the experimental data and the numerical calculations (Fig. 6e–h) confirm that for a thin enough corundum layer the shear zone escapes the corundum and stays excluded from the corundum just above the interface and then returns to the corundum to reach the other corner of the setup. For a critical thickness h_c of the corundum layer the expression (1) has two minima of equal shear force, meaning that there are two optimal configurations: (i) the zone stays in the lower layer or (ii) the zone escapes the lower layer as we have seen for thin layers. These two configurations correspond to the same total force (eqn (1)). For homogeneous pressure this yields

$$h_c = \frac{W}{2}\sqrt{\frac{\mu^h - \mu^l}{\mu^h + \mu^l}},$$

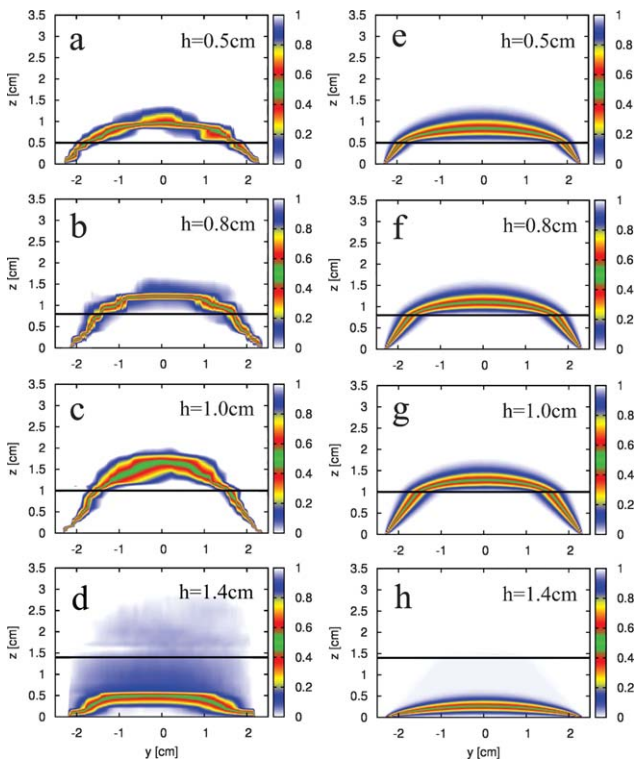

Fig. 6 (a)–(d) Displacement $D(y,z)$ of the material in the *closed system* for four values of the position of the interface $h = 0.5$ cm, $h = 0.8$ cm, $h = 1.0$ cm and $h = 1.4$ cm measured by excavation. (e)–(h) Results of numerical simulations obtained by the fluctuating narrow band model for the same configurations.

where W stands for the width of the cell. For the given cell thickness the estimation for h_c would be 1.1 cm. A similar, but somewhat more complicated calculation that includes hydrostatic pressure and the density difference between corundum and glass beads yields $h_c \approx 1.3$ cm. For thick corundum layers the zone stays in the corundum, for which an example is shown in Fig. 6d at $h = 1.4$ cm. The observations show very nice quantitative agreement with the above calculations, since we find that when h is near the calculated critical thickness, the zone splits up into two branches as it is seen in Fig. 7. This happens at around $h = 1.1$ cm in the experiments and $h = 1.25$ cm in the simulations. The zone is remarkably bent in all cases, which is apparently a direct consequence of the vertical pressure gradient inside the granular material. Namely, frictional forces are smaller at higher levels. Thus eqn (1) results in a curved trajectory even in a homogeneous layer.

Numerous experiments have been carried out using the *closed system*. In Fig. 8 we plot the sine of the angle of incidence as a function of the vertical position h of the interface between the two layers. As it is seen, the measured data match the expected value $1/\sin\beta_c = \mu_h/\mu_l = 1.63$ within experimental error.

Experiments for the *open system* were carried out using both detection methods: excavation and MRI. Several configurations were prepared with different position of the vertically aligned interface. The results of three measurements are shown in Fig. 9 for $y = 0.3$ cm, $y = 0.66$ cm and $y = 0.94$ cm. As it is seen the zone starts from the middle of the cell and moves up toward the right hand side of the sample. Then it leaves the high friction part and continues toward the top surface in the low friction part of the sample. We can calculate the critical distance y_c at which zone splitting is expected in a similar way as we did for the closed system. Here we also take into account that pressure is zero at the top surface and it increases linearly with depth. This yields the critical distance

$$y_c = H\left(\sqrt{\left(\frac{\mu^h}{\mu^l}\right)^2 - 1} - \sqrt{\left(\frac{\mu^h}{\mu^l}\right)^2 - \frac{\mu^h}{\mu^l}}\right),$$

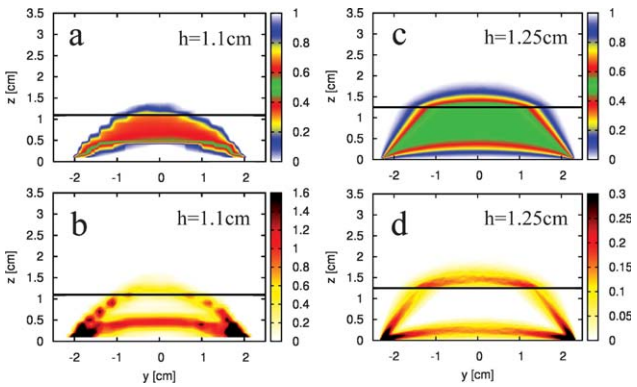

Fig. 7 Splitting of the zone. (a) Displacement $D(y,z)$ and (b) strain in the material in the *closed system* for $h = 1.1$ cm of the position of the interface, measured by excavation. (c)–(d) Results of numerical simulations obtained by the fluctuating narrow band model. In the simulation the splitting of the shear zone occurs at a somewhat higher position of the interface ($h = 1.25$ cm).

 This journal is © The Royal Society of Chemistry 2011

View Online

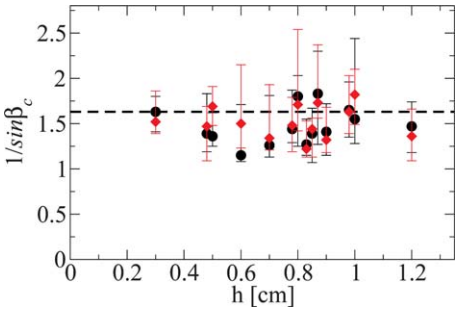

Fig. 8 The sine of the angle of incidence β_c as a function of the vertical position h of the interface between the two layers. Each measurement provides two data points, which are marked with different symbols for clarity. The horizontal dashed line denotes the ratio of the effective friction of corundum and glass beads estimated by angle of repose measurements.

which gives $y_c = 0.93$ for the filling height of $H = 3.4$ cm. The simulation nicely reproduces the splitting of the zone for this configuration (see Fig. 9i) and it is partly visible on the experimental data (Fig. 9c). In case the interface is further away from the center ($y \gg y_c$) we obtain a vertical shear zone in the middle of the cell (not shown here). Then the system behaves as if only the high friction material was present and the interface has no effect on the properties of the shear zone.

Finally, we discuss one difference in the MRI and excavation techniques. While the MRI analysis provides the differential displacement in individual steps, the excavation yields only the integral displacement at the end of the experiment. If the zone position and shape is stationary during the whole experiment, these two informations are equivalent. However, if an initial transient corresponding to the shear zone formation is present, it affects only the excavation data. As the comparison of Fig. 9a–c with Fig. 9d–f shows, this influence plays no role for the present experiments. Nevertheless the quantitative characterization of the initial transient behavior, which is in principle possible with the MRI technique, will be an interesting aspect of future research.

5 Summary

Shear localization in inhomogeneous granular materials has been studied experimentally and numerically. The shear zone preferentially develops in regions with lower friction. In systems consisting of layers with different effective frictions the zone often changes direction at the layer boundary – a phenomenon analogous to light refraction in geometrical optics. The formalism

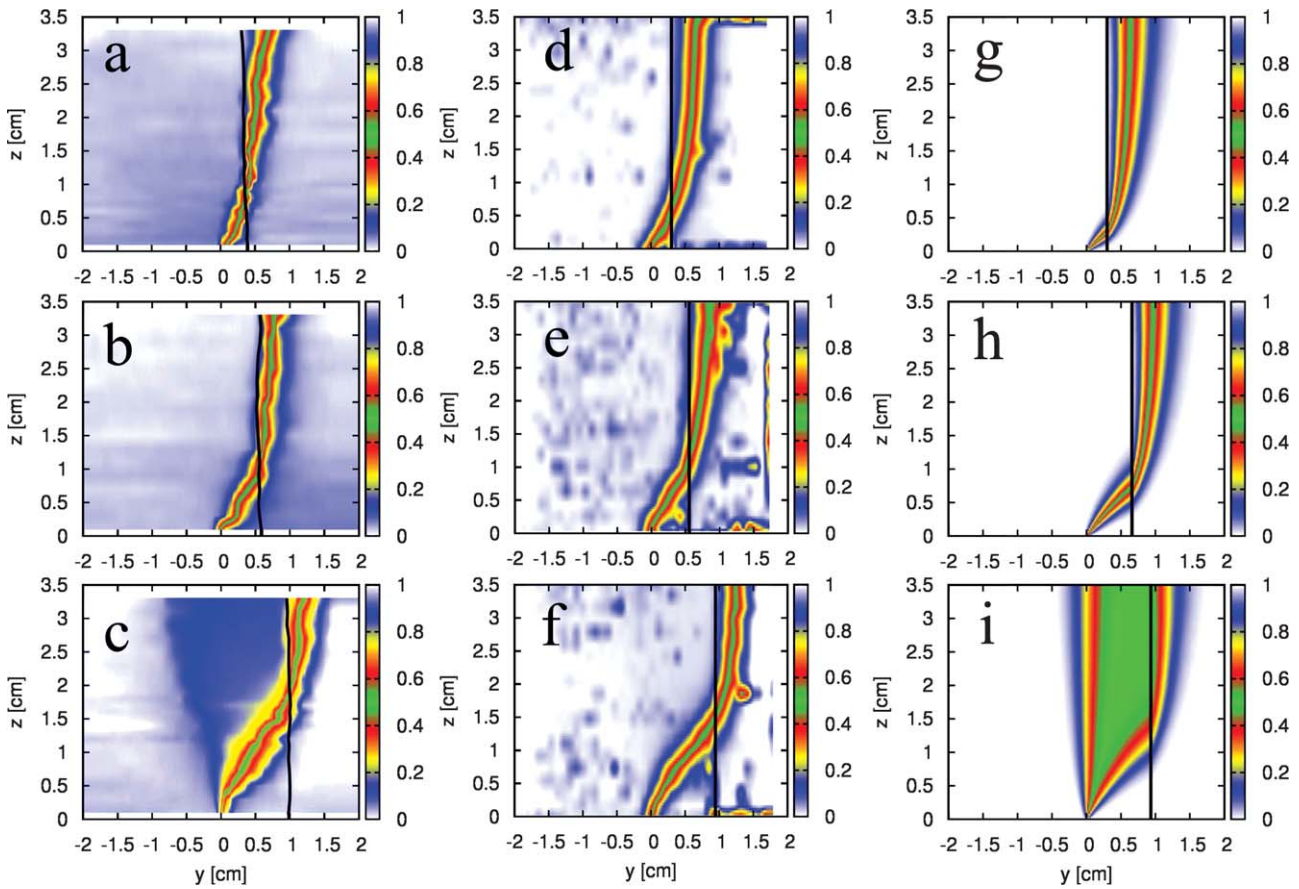

Fig. 9 Displacement $D(y,z)$ of the material in the *open system* for three values of the position of the interface $y = 0.3$ cm, $y = 0.66$ cm and $y = 0.94$ cm measured by (a)–(c) excavation and (d)–(f) magnetic resonance imaging. (g)–(i) Results of numerical simulations obtained by the fluctuating narrow band model for the same configurations.

Downloaded by Otto von Guericke Universitaet Magdeburg on 07 October 2011
Published on 05 August 2011 on http://pubs.rsc.org | doi:10.1039/C1SM05762F

View Online

describing the geometry of the shear zones and that of refracted and reflected light beams is very similar.

Here we have shown that total internal reflection exists also for shear zones. However, unlike in optics the zone reflection occurs always at the critical angle of refraction β_c. In case of shear zones this angle is defined by the ratio of the effective frictions of the two material layers, $\sin \beta_c = \mu_l/\mu_h$. This special reflection also involves a part of the shear zone trapped at the interface of the layers. We expect that such effects are present in naturally layered systems consisting of not only two but multiple layers, and could be best observed if the direction of shear velocity lies parallel while its gradient is perpendicular to the layers. Our measurements also demonstrate that magnetic resonance imaging is a very powerful tool to accurately monitor the internal reorganization of granular materials in quasistatic flows.

Acknowledgements

The authors are thankful for discussions with János Kertész and for technical help from Tilo Finger and André Walther. T.B. and T.U. acknowledge support from the Hungarian Scientific Research Fund (Contract Nos. OTKA F060157 and PD073172).

References

1 J. K. G. Dhont, M. P. Lettinga, Z. Dogic, T. A. J. Lenstra and H. Wang, *Faraday Discuss.*, 2003, **123**, 157.
2 L. B. Chen, C. F. Zukoski, B. J. Ackerson, H. J. M. Hanley, G. C. Straty, J. Barker and C. J. Glinka, *Phys. Rev. Lett.*, 1992, **69**, 688.
3 R. Besseling, E. R. Weeks, A. B. Schofield and W. C. K. Poon, *Phys. Rev. Lett.*, 2007, **99**, 028301.
4 D. Fenistein and M. van Hecke, *Nature*, 2003, **425**, 256.
5 P. Schall and M. van Hecke, *Annu. Rev. Fluid Mech.*, 2010, **42**, 67.
6 D. Fenistein, J. W. van de Meent and M. van Hecke, *Phys. Rev. Lett.*, 2004, **92**, 094301.
7 A. Ries, D. E. Wolf and T. Unger, *Phys. Rev. E*, 2007, **76**, 051301.
8 J. Török, T. Unger, J. Kertész and D. E. Wolf, *Phys. Rev. E*, 2007, **75**, 011305.
9 D. Fenistein, J.-W. van de Meent and M. van Hecke, *Phys. Rev. Lett.*, 2006, **96**, 118001.
10 T. Unger, *Phys. Rev. Lett.*, 2007, **98**, 018301.
11 *Nature Physics, Shear light refraction, Research Highlights*, 2007, 3, p. 76.
12 T. Börzsönyi, T. Unger and B. Szabó, *Phys. Rev. E*, 2009, **80**, 060302R.
13 H. A. Knudsen and J. Bergli, *Phys. Rev. Lett.*, 2009, **103**, 108301.
14 S. Luding, Molecular Dynamics Simulations of Granular Materials, in *The Physics of Granular Media*, ed. H. Hinrichsen and D. E. Wolf, p. 299 (Wiley, 2004).
15 X. Cheng, J. B. Lechman, A. Fernandez-Barbero, G. S. Grest, H. M. Jaeger, G. S. Karczmar, M. E. Mobius and S. R. Nagel, *Phys. Rev. Lett.*, 2006, **96**, 038001.
16 M. Depken, J. B. Lechman, M. van Hecke and W. van Saarloos, *Europhys. Lett.*, 2007, **78**, 58001.
17 M. Depken, W. van Saarloos and M. van Hecke, *Phys. Rev. E*, 2006, **73**, 031302.
18 K. Sakaie, D. Fenistein, T. J. Carroll, M. van Hecke and P. Umbanhowar, *Europhys. Lett.*, 2008, **84**, 38001.
19 E. A. Jagla, *Phys. Rev. E*, 2008, **78**, 026105.
20 D. M. Mueth, G. F. Debregeas, G. S. Karczmar, P. J. Eng, S. R. Nagel and H. M. Jaeger, *Nature*, 2000, **406**, 385.
21 G. D. R. MiDi, *Eur. Phys. J. E*, 2004, **14**, 341–365.
22 T. Unger, J. Török, J. Kertész and D. E. Wolf, *Phys. Rev. Lett.*, 2004, **92**, 214301.
23 T. Börzsönyi, T. C. Halsey and R. E. Ecke, *Phys. Rev. E*, 2008, **78**, 011306.

Downloaded by Otto von Guericke Universitaet Magdeburg on 07 October 2011
Published on 05 August 2011 on http://pubs.rsc.org | doi:10.1039/C1SM05762F

 This journal is © The Royal Society of Chemistry 2011